ELSEVIER

Soil Dynamics and Earthquake Engineering 26 (2006) 221–230

SOIL DYNAMICS AND EARTHQUAKE ENGINEERING

www.elsevier.com/locate/soildyn

Energy approach for earthquake induced slope failure evaluation

T. Kokusho*, T. Ishizawa

Department of Civil Engineering, Chuo University, Tokyo, Japan

Accepted 11 November 2004

Abstract

Earthquake-induced slope stability is evaluated by the force-equilibrium method in engineering practice. This method provides a safety factor against initiating failure or displacement according to the Newmark model along a fixed slip surface but it cannot evaluate failure deformations after failure occurs. An energy approach is proposed as an alternative means for evaluating slope failures and subsequent flow deformations. The driving energy for slope displacement is considered to be the earthquake energy and the gravitational potential energy. As a first step in the research, an energy balance is formulated for the model of a rigid block resting on an inclined plane. Then, an innovative model test is developed, in which the energy balance in a sliding slope is measured on a shake table. The earthquake energy used for the slope failure can be successfully quantified in the test and its contribution to displacement is discussed in the light of the energy balance established for the block model.

Keywords: Earthquake energy; Energy dissipation; Shaking table test; Residual slope deformation

1. Energy approach

Seismically induced slope failures have normally been evaluated based on the equilibrium of forces acting on a potentially sliding soil mass. This force approach can evaluate the initiation of slide or the safety factor against the slope failure, but it cannot predict slide deformations, once failure occurs. From the viewpoint of the performance based design or the risk evaluation of slope failures, it is very important to evaluate not only the safety factor, but also how large the deformation will develop and how far the effect reaches down-slope. The Newmark method [1] can evaluate slope displacement along a fixed slip surface based on a double integration of acceleration of a potentially sliding soil block. The same acceleration is assumed in the sliding block as on the slope. Makdisi and Seed [2] modified the original method to deal with the acceleration amplification in soil structures by using FEM analyzes. The Newmark method or its modifications have often been used in a slope stability analysis for dams and important structures. Finn [3] summarized the engineering practice for evaluating the seismic safety of embankment dams and wrote that the method is widely used despite all the evidence that the sliding block model is not a very good representation of how embankment dams deform, especially embankment dams with low factors of safety.

The Newmark method seems to result in smaller slope deformations because of the assumptions that the sliding soil mass is rigid and soil strength is fixed. In actual slope failures, sliding soil may not always behave as a rigid body but deforms continuously without distinct slip surfaces. It sometimes tends to become destructive due to a shift from slow slide to fast flow because the soil strength decreases drastically after the initiation of failure.

In this research, an energy approach is proposed to evaluate slope failures including flow failures from their initiation to termination. The basic idea, first proposed in [4], is shown in Fig. 1.

There are several different causes triggering slope failures; such as earthquakes, heavy rainfalls, artificial cutting or banking, etc. These causes may increase the driving force and/or decrease the soil strength in different ways.

In case of earthquake-induced slope failures, four energies; potential energy due to gravity E_p, kinetic energy E_k of sliding soil mass, earthquake energy contributing to

* Corresponding author. Tel.: +81 3 3817 1798; fax: +81 3 3817 1803.
E-mail address: kokusho@civil.chuo-u.ac.jp (T. Kokusho).

0267-7261/$ - see front matter © 2005 Elsevier Ltd. All rights reserved.
doi:10.1016/j.soildyn.2004.11.026

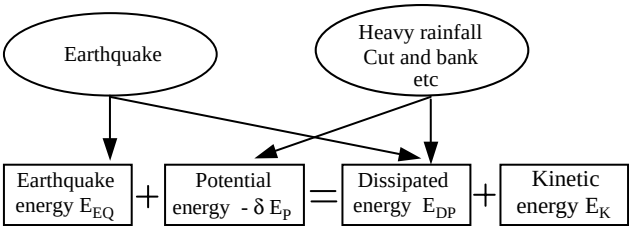

Fig. 1.

the slope failure E_{EQ} and energy dissipated in the soil due to the slope deformation E_{DP}, can be correlated by the following equation

$$E_{DP} + E_k = E_{EQ} - \delta E_p \tag{1}$$

or in incremental form as:

$$\Delta E_{DP} + \Delta E_k = \Delta E_{EQ} - \Delta\delta E_p \tag{1'}$$

Note that the potential energy change due to failure, δE_p in Eq (1) or $\Delta\delta E_p$ in Eq. (1′) is normally negative. If failures occur after the end of earthquake shaking as often observed in case histories, the energy balance becomes identical with that in slope failures due to rainfall or other non-seismic causes without the earthquake energy:

$$\Delta E_{DP} + \Delta E_k = \Delta\delta E_p \tag{2}$$

In non-seismic cases, if $-\Delta\delta E_p$ is larger than ΔE_{DP} in Eq. (2), then $\Delta E_k > 0$ and failure starts. Namely, the condition for initiation of failure is:

$$\Delta E_k = -\Delta\delta E_p - \Delta E_{DP} > 0 \text{ or } -\Delta\delta E_p > \Delta E_{DP} \tag{3}$$

Once failure starts, the amount of the dissipated energy is critical to decide if it develops as a flow-type failure and to determine how far it flows. If ΔE_{DP} is smaller than $-\Delta\delta E_p$ in some time increments, then ΔE_k is increased and the soil movement is accelerated. A shift from slow slide to fast flow may occur not only due to increase in $-\Delta\delta E_p$ but also due to drastic decrease of ΔE_{DP} caused by pore-pressure buildup in liquefiable soil, strength loss in high-sensitivity clay, etc. In fast flow failures, the soil mass can keep flowing unless the kinetic energy at a time (E_k) plus the subsequent potential energy change ($-\delta E_p$) is all dissipated.

If $-\Delta\delta E_p$ is smaller than ΔE_{DP}, then ΔE_k is negative, hence the soil mass decreases the speed and comes to a halt if reserved kinetic energy E_k is all consumed. If the failure mode and the energy dissipation mechanism in flowing soil mass are known, it is possible to evaluate how far the flow will reach in the down-slope direction [4].

2. Energy approach to Newmark method

The original Newmark Method [1] or modifications of it are commonly used in geotechnical earthquake engineering practice to estimate seismically induced displacement of earth-structures. The original method considered a soil block on a horizontal slip plane but it can be applied also to a block on an inclined plane or a curved surface [5].

Let us assume a block of mass M on a slip plane subjected to a horizontal seismic coefficient k. The displacement of the block is s along the slope and δ_r in the horizontal direction. If the slip plane is inclined by 1 to β from horizontal:

$$\delta_r/s = 1/(1+\beta^2)^{1/2} \tag{4}$$

Normal and tangential components of the block weight N and T, shown in Fig. 2, are:

$$N = (1-\beta k)Mg/(1+\beta^2)^{1/2} \tag{5}$$

$$T = (\beta + k)Mg/(1+\beta^2)^{1/2} \tag{6}$$

From the equilibrium of forces along the slope

$$-M\frac{d^2s}{dt^2} - Mg\mu\frac{1-\beta k}{(1+\beta)^{1/2}} + Mg\frac{\beta+k}{(1+\beta)^{1/2}} = 0 \tag{7}$$

where $\mu = \tan\phi$ is the friction coefficient between the slope and the block, and ϕ is the friction angle. If the horizontal seismic coefficient k is sustained during the time interval $t = 0$–T and the initial velocity of the block is zero, time-dependent changes of relative velocity and relative displacement of the block are obtained as shown in Fig. 3. The relative velocity and displacement at $t = T$ are

$$v_T = \frac{ds}{dt}|_{t=T} = \frac{(1+\mu\beta)}{(1+\beta^2)^{1/2}}(k-k_{cr})gT \tag{8}$$

$$s_T = \frac{(1+\mu\beta)}{2(1+\beta^2)^{1/2}}(k-k_{cr})gT^2 \tag{9}$$

where

$$k_{cr} = \frac{\mu-\beta}{1+\mu\beta} \tag{10}$$

is the critical seismic coefficient, and slip occurs only when $k > k_{cr}$. The final block displacement s_0 is

$$s_0 = \frac{k}{k_{cr}}s_T \tag{11}$$

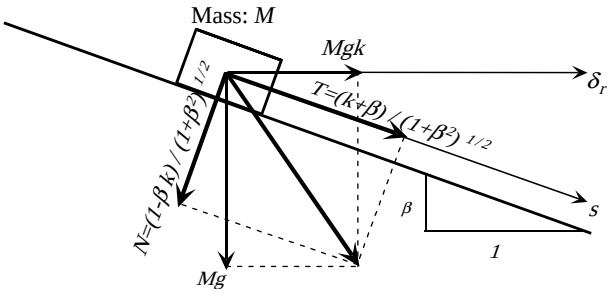

Fig. 2. A block on a slope subjected to seismic effect.

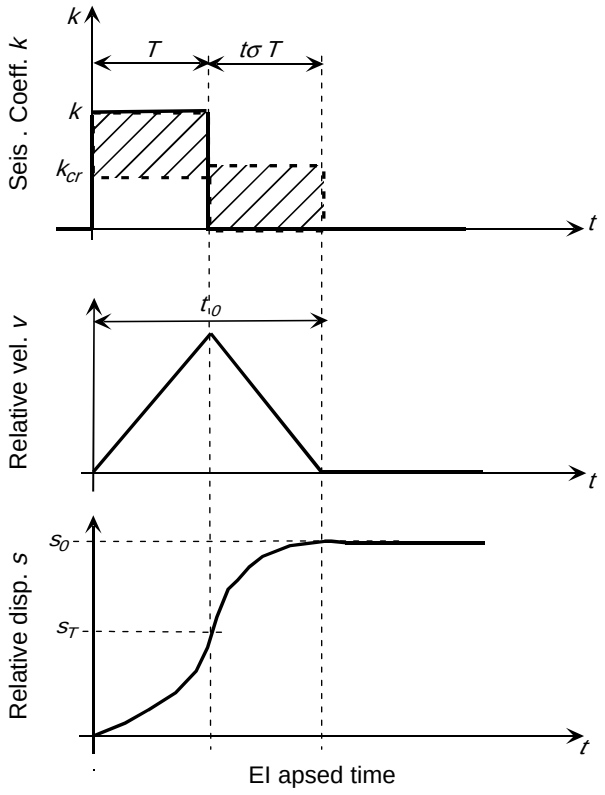

Fig. 3. Time dependent change of seismic coefficient k, relative velocity v and relative displacement s of the block along the slope.

and it occurs when

$$t_0 = \frac{1+\mu\beta}{\mu-\beta}kT \tag{12}$$

In terms of energy, the potential energy change δE_p for the block slippage of distance s_0 along the slope is:

$$\delta E_p = -Mg\beta\delta = -\frac{\beta}{(1+\beta^2)^{1/2}}Mgs_0 \tag{13}$$

The dissipated energy E_{DP} which occurs exclusively along the slip plane in the rigid block model is expressed as:

$$E_{DP} = \frac{\mu(1+\beta k)}{(1+\beta^2)^{1/2}}Mgs_T + \frac{\mu}{(1+\beta^2)^{1/2}}Mg(s_0 - s_T)$$

$$= \frac{\mu(1+\beta^2)^{1/2}}{1+\mu\beta}Mgs_0 \tag{14}$$

From Eq. (1), the earthquake energy contributing to block slippage is

$$E_{EQ} = E_{DP} + \delta E_p = \frac{(\mu-\beta)}{(1+\mu\beta)}Mg\delta_r \tag{15}$$

where the kinetic energy E_k is zero after slope movement ceases.

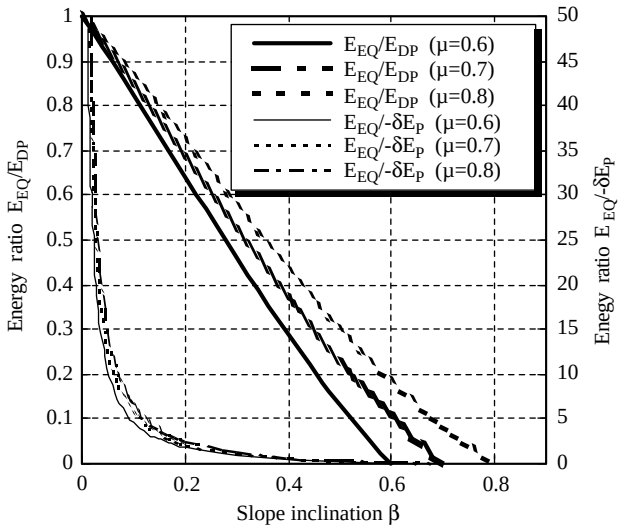

Fig. 4. Energy ratios E_{EQ}/E_{DP}, $E_{EQ}/\delta E_P$ versus β relationship.

The ratios of E_{EQ} to E_{DP} and E_{EQ} to $-\delta E_p$ are:

$$\frac{E_{EQ}}{E_{DP}} = \frac{(\mu-\beta)}{\mu(1+\beta^2)} \tag{16}$$

$$\frac{E_{EQ}}{-\delta E_p} = \frac{(\mu-\beta)}{\beta(1+\mu\beta)} \tag{17}$$

In Fig. 4, the relationship of E_{EQ}/E_{DP} or $E_{EQ}/-\delta E_p$ versus the slope inclination β is shown. It is clear that the ratios of earthquake energy to dissipated energy and potential energy are totally independent of seismic coefficient k and depends only on slope inclination β and friction coefficient μ. Also note that the contribution of E_{DP} becomes smaller with larger slope inclination β and smaller friction coefficient μ.

The block model on the slip plane, captures basic physics of the slope failure mechanism, but cannot reproduce the failure of the sloping soil mass. One of the most significant differences may be that, in actual slope failures, soil mass does not slide as a rigid body along a fixed slip plane but deforms continuously with or without movable slip planes. Furthermore, if the friction coefficient μ reduces due to pore pressure buildup or other mechanisms after the initiation of failure or soil mass moves without any distinct slip plane, it cannot predict the displacement of the failed soil mass anymore. Consequently, a model slope consisting of dry sand is tested on a shake table to quantify energies involved in the slope failure more realistically than the Newmark-type model.

3. Shake table model tests

A spring-supported shaking table shown in Fig. 5 was utilized to apply vibrations to a model slope made from sand, called Model-A here, in a rectangular lucite box.

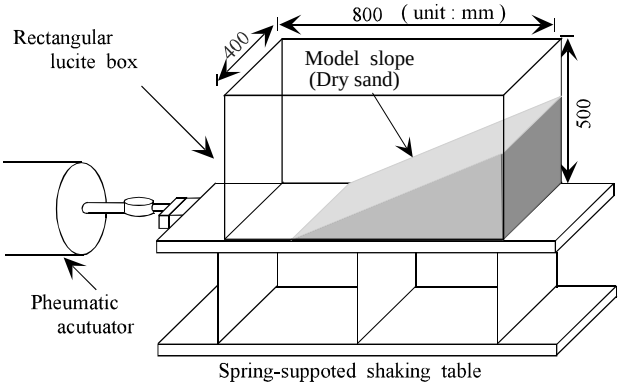

Fig. 5. Shake table test apparatus for model slopes.

The model slope (base length; $L=60$ cm, height; $H=33$ cm, width; $B=40$ cm) was made by air-pluviating dry clean Toyoura sand to a prescribed relative density of Dr$\approx$40%. The slope angle was about 29°. In order to evaluate the friction coefficient μ of the model slope, the slope was gradually inclined statically until the onset of slope failure. The static tests carried out three times with the same initial slope angle of 29° and Dr$\approx$40% gave the angle of repose 34.8–36.0° (average 35.3).

The table was initially pulled to a prescribed horizontal displacement and then released to generate damped free vibration. Dissipated energy, which can be calculated from the decay in displacement amplitude in each cycle depends not only on the energy dissipation due to slope deformation but also on other energy loss mechanisms such as radiation damping in the shake table foundation. In order to extract the dissipated energy due to slope deformation, a dummy model, called Model-B consisting of a pile of rigid concrete blocks, was made in the same lucite box and vibrated in the same way as shown in Fig. 6. The total weight and the center of gravity were adjusted to be almost identical in the two models.

The decay in amplitudes, measured by a LVDT displacement gauge in both Models-A and -B are shown in Fig. 7. Notes that, though the initial table displacement, 2.0 cm, and the vibration period of the table, 0.19 s, are almost the same, the difference in amplitudes grows larger with increasing number of cycles. It may be reasonable to assume that this difference reflects the greater energy dissipated in Model-A (the model slope) due to its internal deformations, since almost negligible energy is dissipated in the rigid concrete blocks in Model-B.

Fig. 8 exemplifies the damping ratio D versus the number of cycles N relationship calculated from the decay vibrations of Models-A and -B. Here, D is calculated by the following equations

$$D = \frac{1}{2\pi}\ln\frac{u_i}{u_{i+1}} \tag{18}$$

where u_i and u_{i+1} are displacement amplitudes of the ith cycle and $(i+1)$th cycle, respectively. The differences in D between the two models are clearly recognizable.

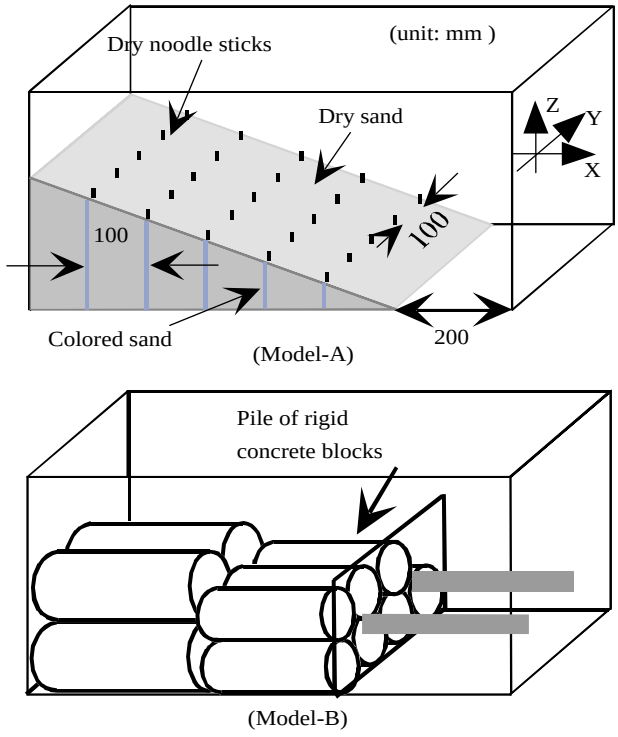

Fig. 6. Dry sand model slope (Model-A) versus concrete block pile (Model-B) of the same weight and centroid.

The loss energy per cycle ΔW can be calculated as

$$\Delta W = 4\pi WD \tag{19}$$

in which W, representing the strain energy in the same cycle, can be evaluated from the spring constant κ and the displacement amplitudes of the shaking table as:

$$W = \frac{1}{2}\kappa\left(\frac{u_i + u_{i+1}}{2}\right)^2 \tag{20}$$

Fig. 9 shows the force versus displacement relationship of the shake table when it is pulled by static force. It may be

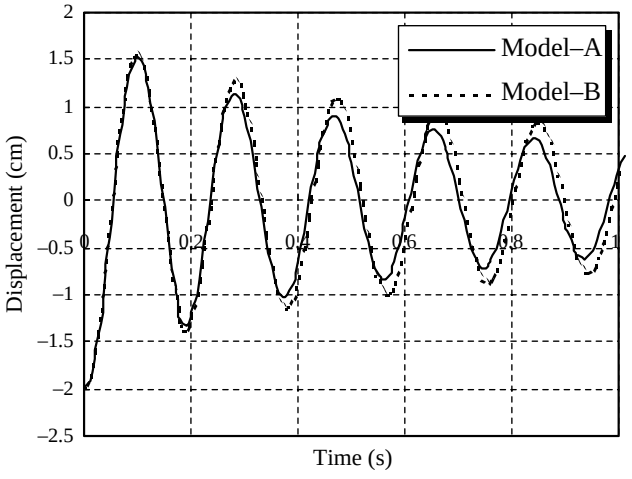

Fig. 7. Decay vibrations measured by a LVDT displacement gauge in the Models-A and -B.

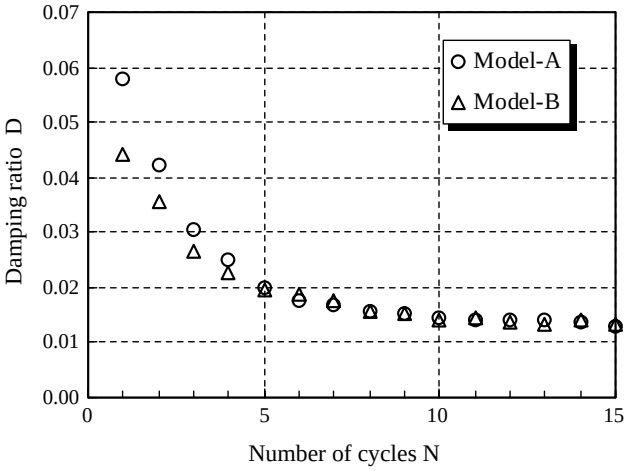

Fig. 8. Damping ratio D versus number of cycles N relationship calculated from decay vibrations of Models-A and -B.

approximated by a straight line from which the spring constant κ can be evaluated.

The earthquake energy increment in the model slope ΔE_{EQ} can then be evaluated from the loss energies per cycle in Models-A and -B, ΔW_A and ΔW_B, respectively as:

$$\Delta E_{EQ} = \Delta W_A - \Delta W_B \tag{21}$$

In Fig. 10, the loss energy in Model-B, ΔW_B, evaluated by four tests of the same test condition is plotted versus the average table amplitude $(u_i + u_{i+1})/2$. It may be noted that the results, which show good reproducibility with minimal data dispersion, can be represented by the average curve in the chart. In Fig. 11, ΔW_A evaluated for one of the tests on Model-A is compared with the average curve of ΔW_B. The difference ΔE_{EQ} calculated by Eq. (21) for each cycle is also plotted on the same chart, indicating that ΔE_{EQ} reduces to almost zero after around sixth cycle. This is consistent with

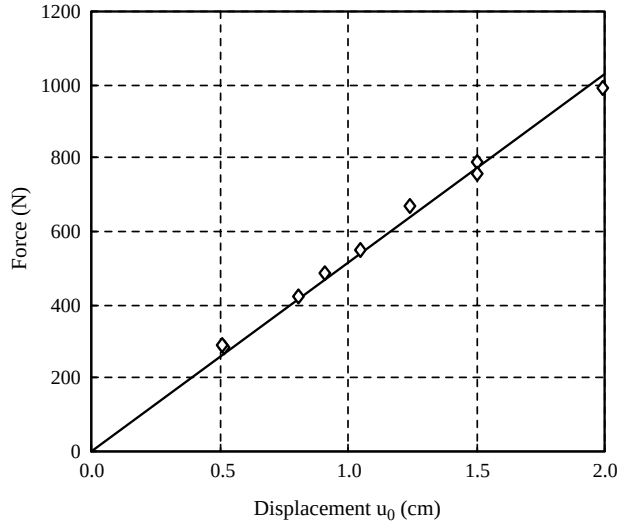

Fig. 9. Force versus displacement relationship of the shake table by a static pulling force.

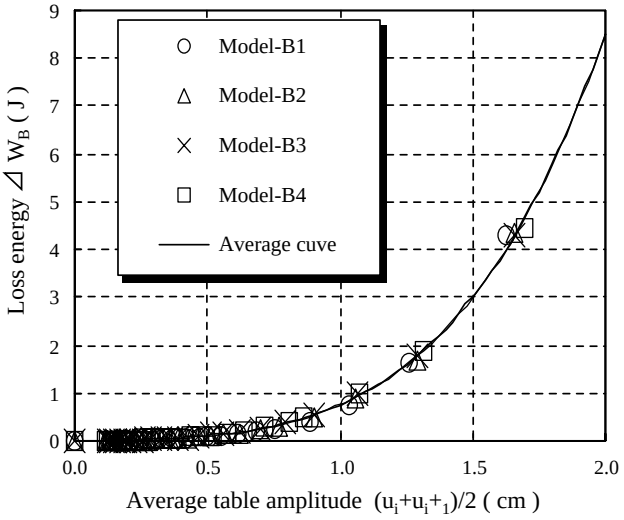

Fig. 10. Loss energy in Model-B versus the average table amplitude.

the experimental observation that the residual deformation of the model slope was visible only within first 5 cycles. The total earthquake energy E_{EQ} calculated as a sum of ΔE_{EQ} in each cycle represents the amount of earthquake energy involved in producing the final displacement in the model slope. To be more precise, E_{EQ} also includes the energy dissipated by soil damping in the model during vibration, which is neglected in the interpretation of the model test results. The total input energy applied to the shaking table E_{IP} can be calculated from the initial pull displacement u_0 of the table as:

$$E_{IP} = \frac{1}{2}\kappa u_0^2 \tag{22}$$

The relationship between E_{EQ} and E_{IP} shown in Fig. 12 indicates that the ratio E_{EQ}/E_{IP} tends to decrease slightly with increasing input energy but it may be approximated by

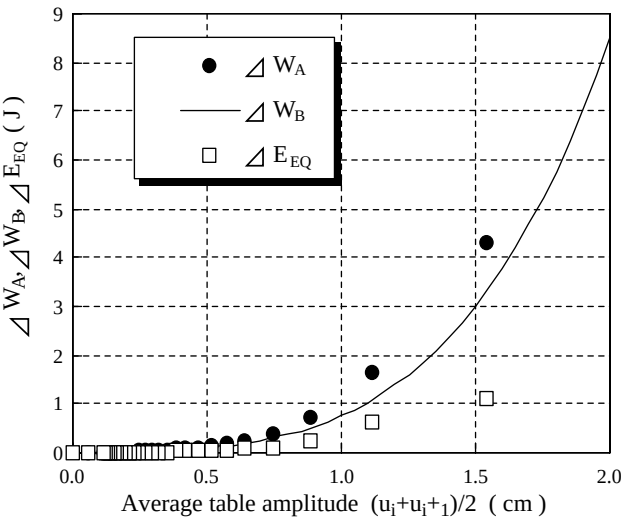

Fig. 11. Dissipated energy obtained as a difference of loss energies in Models-A and -B.

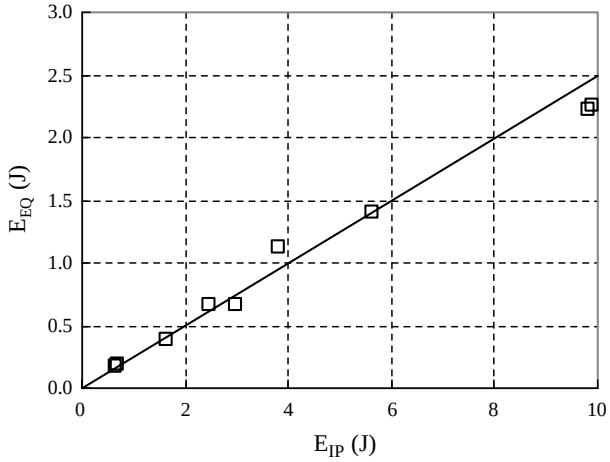

Fig. 12. Relationship between earthquake energy actually used for slope deformation E_{EQ} to the total earthquake energy E_{IP}.

the straight line of $E_{EQ}/E_{IP}=0.25$. It indicates that the fraction of the earthquake energy actually used for slope failure may be assumed almost constant no matter how large the input seismic energy is or how much slope failure occurs.

4. Slope deformation

The deformation of the model slope was observed by two video cameras, one from the side and the other from above. Column-shaped markers made from colored sand were installed at the side of the model. On the slope face, dry noodle sticks of 5 cm length were set up in line. The interval of these markers was 10 cm in the slope direction. The slope deformation was also measured by a laser beam displacement sensor.

In Fig. 13(a) movements of the vertical markers made from colored sand at each cycle from the start to the fifth cycle of the test are shown. Note that the slope deforms continuously in the down-slope direction and also discontinuously accompanying clear slip surfaces in the middle part of the slope length. The cycle-by-cycle surface change of the slope measured by the laser sensor combined with the video movie is also shown in the same figure. It indicates height decease in the upslope side and increase in the down-slope side and also some volume contraction during the slope failure. In Fig. 13(b), a plan view of the movement of markers on the slope surface is shown from the start to the end of the test, indicating that the deformation may be approximated to be uniform in the direction normal to the cross-section. In order to correlate the energies with the residual displacement of the slope, the horizontal residual displacement δ_r (which is converted to the displacement along the slope, s, by Eq. (4)) was evaluated as an average of the spatially variable measurements. To explain more in detail, δ_r was calculated as the average of averaged horizontal displacements along all vertical markers above

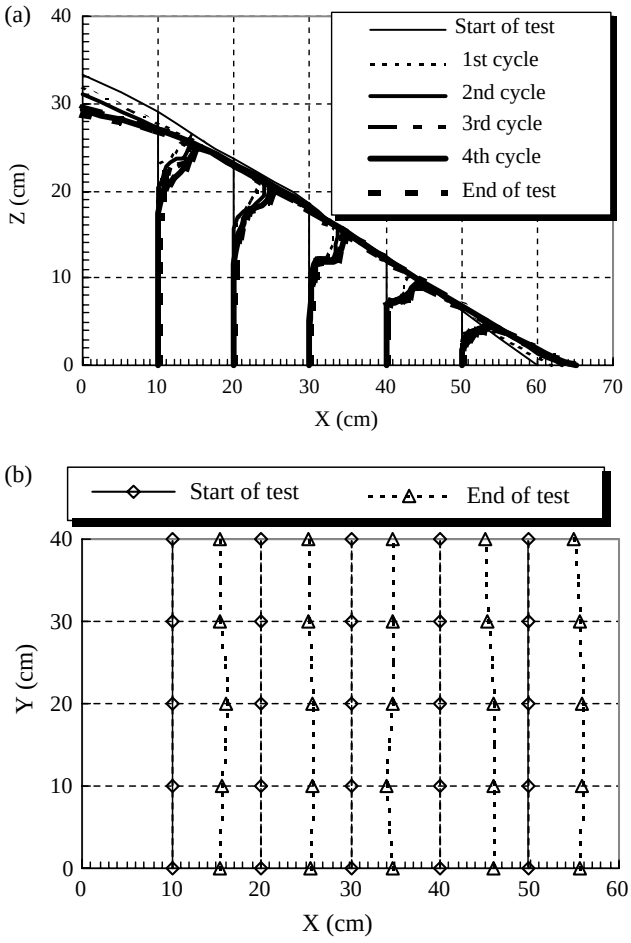

Fig. 13. (a) Movement of markers from side. (b) Movement of markers at the slope surface from above.

the deepest points where the deformation was observed as shown in Fig. 14. The uniformity of the slope displacement was assumed in the direction normal to the cross-section. This calculation was implemented in each cycle of the input vibration to obtain the incremental residual displacement $\Delta\delta_r$.

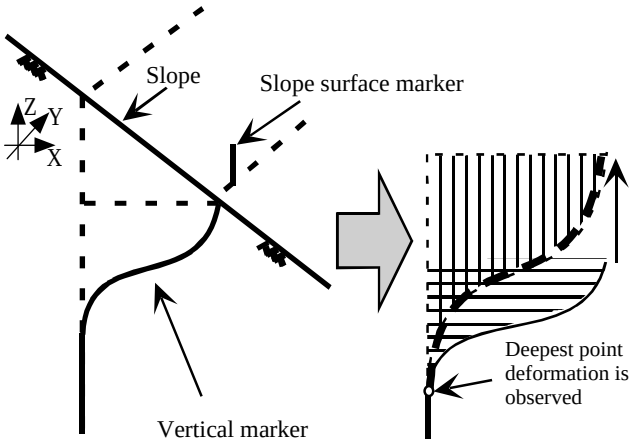

Fig. 14. Evaluation of averaged horizontal displacements $\Delta\delta_r$ of slope.

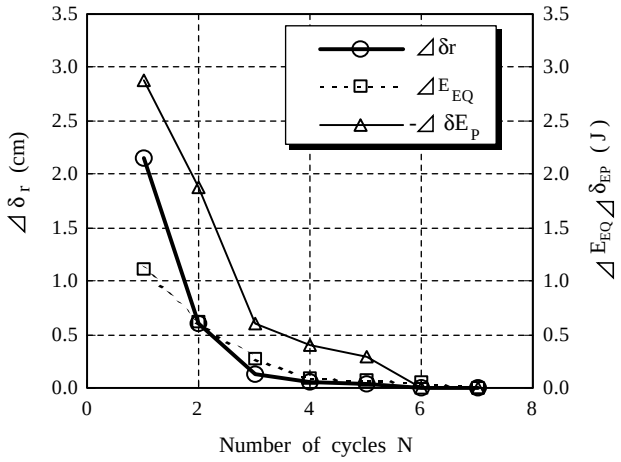

Fig. 15. Displacement $\Delta\delta_r$, incremental energies, ΔE_{EQ} and $-\Delta\delta E_p$ plotted versus the number of cycles N.

In Fig. 15, $\Delta\delta_r$ is plotted versus the number of cycles, N. The incremental earthquake energy $-\Delta E_{EQ}$ and the potential energy change $-\Delta\delta E_p$ are also plotted against N in the same chart. From the change in the slope surface geometry $-\Delta\delta E_p$ is calculated cycle by cycle as

$$\Delta\delta E_p = \Delta(\rho_d g B \int z\,dx dz) \tag{23}$$

where z is the vertical coordinate, ρ_d is the dry soil density and assumed constant. The integration is carried out over the cross-sectional area of the slope. It is again confirmed that measurable slope deformation occurs only until about fifth cycle, which is almost consistent with the variation in the earthquake energy ΔE_{EQ}.

5. Slope displacement versus energy

It may be assumed here that the kinetic energy ΔE_k in Eq. (1′) is small and ignorable because the velocity of displaced soil mass is not large in this test. Hence:

$$\Delta E_{DP} = \Delta E_{EQ} - \Delta\delta E_p \tag{24}$$

In Fig. 16, the increment of average horizontal slope displacement $\Delta\delta_r$ in each cycle is correlated with corresponding ΔE_{DP} evaluated by Eq. (24) for several tests conducted for the same model with different initial table displacements. The correlation is not linear but convex in all tests. This may indicate that some mechanism is involved in which the energy dissipation per unit incremental residual displacement tends to be smaller for larger $\Delta\delta_r$.

The incremental energies, ΔE_{EQ}, $-\Delta\delta E_p$ and ΔE_{DP} calculated in each cycle are summed up from the first to 5th cycle to evaluate the corresponding total energies, E_{EQ}, $-\delta E_p$ and E_{DP}. In Fig. 17, the values of $-\delta E_p$ and E_{DP} are plotted versus the earthquake energy E_{EQ} for several test cases with different initial table displacements. According to the dashed line approximating the plots of $-\delta E_p$ versus

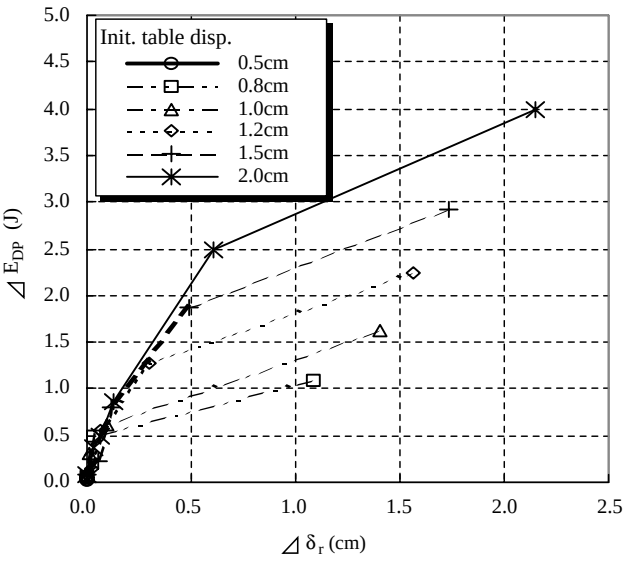

Fig. 16. Relationships between incremental dissipated energy ΔE_{DP} and incremental residual displacement $\Delta\delta_r$ for several test cases with different initial table displacement.

E_{EQ}, it is obvious that the potential energy change $-\Delta\delta E_p$ contributes about three times more to the slope failure than the earthquake energy ΔE_{EQ}, although the latter serves as the trigger of the slope failure because the slope of the model is relatively large.

In the light of the energy considerations on the Newmark Model discussed before and summarized in Fig. 4, the ratios E_{DP}/E_{EQ} and $-\delta E_p/E_{EQ}$ can be calculated theoretically by Eqs. (16) and (17) based on the rigid block model. Because the angle of the slope is 29° ($\beta=0.55$) and the angle of repose of the sand is about 35° ($\mu=0.70$), $E_{DP}/E_{EQ}=6.1$ and $-\delta E_p/E_{EQ}=5.1$. These two relations are drawn in Fig. 17

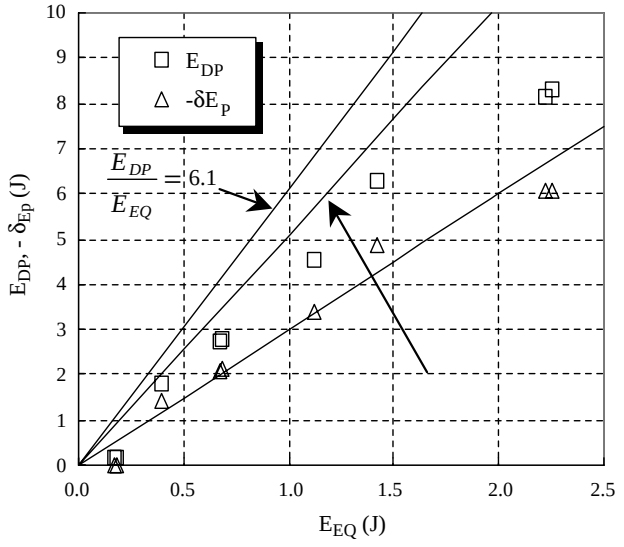

Fig. 17. Earthquake energy E_{EQ} plotted versus potential energy or dissipated energy for several test cases with different initial table displacement.

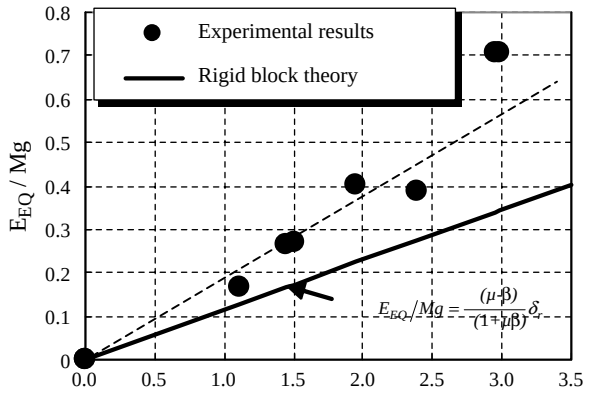

Fig. 18. Relationships between residual displacement δ_r and earthquake energy E_{EQ}/Mg for different initial table displacements compared with the rigid block theory.

by two solid lines. Obviously, there is a wide gap between the theory on the rigid body model and the sand slope. However, the experimental results may also be roughly approximated by straight lines, indicating that $-\delta E_p$ and E_{DP} tend to increase almost in proportion with E_{EQ} irrespective of the intensity of shaking.

In Fig. 18, the residual displacement δ_r at the end of shaking obtained by several tests with different initial table displacement are plotted versus the normalized earthquake energy E_{EQ}/Mg, where the weight of the displaced soil mass was evaluated in video pictures of individual tests. The solid straight line indicates the theoretical relationship by the rigid block model indicated in Eq. (15) for $\beta=0.55$ and $\mu=0.70$, in which the displacement δ_r is proportional to the normalized earthquake energy. Note that obviously larger energy is needed in the model test than the theory for the same slope displacement. This discrepancy may reflect the difference of failure mechanism between the continuous soil slope and the simplified block model.

6. Performance based slope evaluation by energy approach

Based on the theoretical considerations on the simplified block model and the model test explained above, a framework for performance based design in which residual slope displacements are to be evaluated during earthquakes may be proposed as follows.

First, the input earthquake energy E_{IP} defined at the base of slopes or embankments is designated site by site as shown in Fig. 19. The energy E_{IP} can be evaluated [6] from the integration of the square of the particle velocity of the design motions du/dt in terms of time t times the impedance of the base layer $\rho_2 Vs_2$ as:

$$E_{IP} = \rho_2 Vs_2 \int (du/dt)^2 dt \tag{25}$$

By assuming the energy radiating downward through the base, E_d, the earthquake energy, E_{EQ}, which can be consumed inside the slopes or embankments can be obtained as:

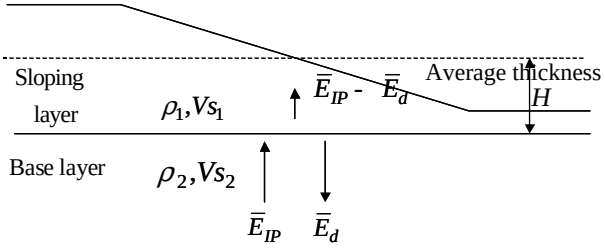

Fig. 19. Definition of seismic wave energy at the base of a sloping layer.

$$E_{EQ} = E_{IP} - E_d \tag{26}$$

In the present model test, $E_{EQ}/E_{IP}=0.25$ could be assumed despite the difference of slope displacement according to Fig. 12.

Theoretically, the energy ratio is controlled by the impedance ratio $\alpha=\rho_1 Vs_1/\rho_2 Vs_2$ between the sloping ground and a base layer as illustrated in Fig. 19. Here a sloping ground is approximated by a horizontal two-layers system with the average height H in the upper layer. Under stationary vibration by sinusoidal input motion, the ratio between the energy flux of downward radiation wave $\bar{E}_d$ and that of upward input wave $\bar{E}_{IP}$ can be formulated as Eq. (26) based on the one-dimensional SH wave propagation [6]. Here, the energy flux means the amount of harmonic wave energy transmitted in a unit time:

$$\bar{E}_d/\bar{E}_{IP} = \left|\frac{(1-a^*)+(1+a^*)e^{-2ik_1^* H}}{(1+a^*)+(1-a^*)e^{-2ik_1 H}}\right|^2 \tag{27}$$

Here, $k_1^* = \omega/Vs_z^*$ (ω is the angular frequency) and complex impedance ratio α^* can be written as

$$\alpha^* = r_1 Vs_1^*/r_2 Vs_2^* = \alpha\{(1+2iD_1)/(1+2iD_2)\}^{1/2} \tag{28}$$

in which Vs_1^*, Vs_2^*, complex S-wave velocity and D_1; D_2, damping ratios of the upper and lower layer, respectively. If the energy flow is stationary by harmonic wave propagation, the energy stored in the sloping layer is $W=\bar{E}_{IP}-\bar{E}_d$ and the energy dissipating downward by radiation is $\Delta W=\bar{E}_d$. From an analogous expression for a lumped mass linear viscous system which is in resonance with a harmonic input motion, the damping ratio due to wave radiation D_r may be defined as:

$$D_R = \Delta W/4\pi W = \bar{E}_d/4\pi(\bar{E}_{IP}-\bar{E}_d) \tag{29}$$

Consequently, the energy flux ratio $\bar{E}_d/\bar{E}_{IP}$ can be correlated with the radiation damping ratio D_r as:

$$\bar{E}_d/\bar{E}_{IP} = 4\pi D_R/(1+4\pi D_R) \tag{30}$$

If Eq. (29) can also be assumed for transient earthquake waves then:

$$E_d/E_{IP} = 4\pi D_R/(1+4\pi D_R) \tag{30'}$$

The rest of the energy $E_{EQ}=E_{IP}-E_d$ is the maximum energy which can potentially be used for

deformation and failure of the sloping ground. If, for instance $D_r=15\%$ as sometimes used in embankment dams in Japan, then, $E_d/E_{IP}=0.65$ and $E_{EQ}/E_{IP}=0.35$.

More practically, the energy ratio E_{EQ}/E_{IP} may be quantified by FEM analyzes and the radiation damping effect is considered by transmitting boundaries or dashpots. Design input motions are given at the base layers and the motions at the levels of the estimated slip plane are computed.

Of course, E_{EQ} varies along the layer boundary in two dimensional problems and some averaging process may be needed.

The energy E_{EQ} is dissipated by residual slope deformation as well as by internal soil damping in the sloping layer. The present model tests indicate that the energy by internal damping E'_{EQ} seems small compared to E_{EQ}. If necessary, it is possible to evaluate the energy E'_{EQ} associated with internal soil damping based on FEM analyzes and thus the earthquake energy to be used for the residual slope deformation $(E_{EQ}-E'_{EQ})$ can be differentiated.

Based on the rigid block simple model, the residual horizontal displacement is expressed based on Eq. (15) as:

$$\delta_r=\frac{(1+\mu\beta)}{(\mu-\beta)}\frac{E_{EQ}-E'_{EQ}}{Mg} \tag{31}$$

The thickness or the mass of sliding soil may be determined by conventional slip surface analyzes. As previously mentioned for Fig. 18, the test results may be approximated by a dashed line 70% steeper than the theoretical line, indicating the rigid block model may be applicable by modifying the friction constant μ. This is probably because the model slope consists of non-liquefiable dry sand (Fig. 20).

Whenever there were severe damage by seismically induced slope failures or landslides, soil strength seems to have drastically decreased due to pore pressure buildup or some other reasons. In order to take such unstable soils into considerations, the coefficient $(1+\mu\beta)/(\mu-\beta)$ in Eq. (31) should be modified in accordance to field performance in previous slope failures.

These are merely the essence of the slope evaluation procedures by the energy approach. Much more work by model tests, case history studies, etc. is still needed to establish reliable evaluation tool for slope displacements based on the energy approach.

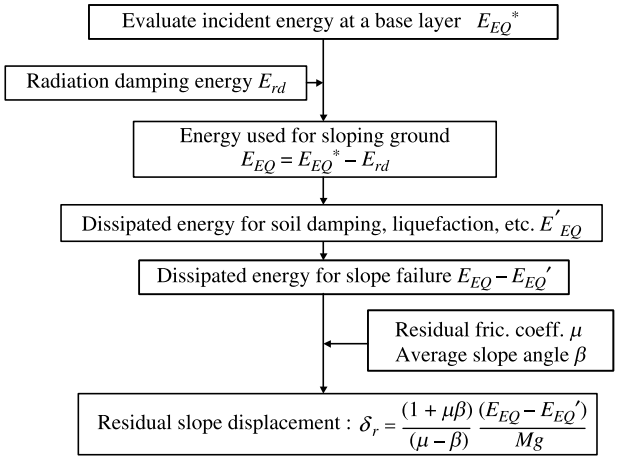

Fig. 20. Flow chart for evaluation of slope displacement by energy approach.

7. Conclusions

The energy approach has been applied to slope failure evaluation first by examining the energy balance in the Newmark-type block model and then by carrying out an innovative shake table tests of a model slope of dry sand, yielding the following major findings.

(1) The energy balance in the block model indicates that the ratio of the earthquake energy used for slope failure E_{EQ} to the energy dissipated in the slope E_{DP} is independent of seismic coefficient k and depends only on slope inclination β and friction coefficient μ. E_{EQ} becomes smaller with larger β and smaller μ. The slope displacement is formulated to be proportional to E_{EQ}.
(2) The earthquake energy used for slope failure E_{EQ} can be successfully measured in the innovative model test developed in this research, quantifying the energy balance involved in the failure of the model slope.
(3) The contribution of the earthquake energy E_{EQ} is smaller than the potential energy in this test, because the slope angle 29° is high enough to be comparable to the angle of repose which is about 35°. The energy analysis on the rigid block model indicates that the lower the slope angle, the higher the contribution of earthquake energy in comparison with the potential energy.
(4) In the relationship between the residual slope displacement δ_r and the earthquake energy, obviously larger energy is needed in the model test than the theory for the same slope displacement. This discrepancy may reflect the difference of failure mechanism between the continuous soil slope and the simplified block model.

Based on the above results, a framework for the energy approach for evaluating slope deformation in practical designs has been proposed. In order to upgrade this approach to a reliable design tool, more research on the energy balance in complex in situ conditions is needed.

References

[1] Newmark NM. Effects of earthquakes on dams and embankments. Fifth Rankine Lecture, Geotechnique, vol. 15; 1965, p. 139–59.

[2] Makdisi FI, Seed HB. Simplified procedure for estimating dam and embankment earthquake-induced deformations. J Geotech Eng Div ASCE 1978;104(GT7):849–67.

[3] Liam Finn WD. North American practice for evaluating the seismic safety of embankment dams. Proceedings of the first international conference on earthquake geotechnical engineering, IS-Tokyo, 95, vol. 3; 1995, p. 1227–52.

[4] Kokusho T, Kabasawa K. Energy approach to flow failure and its application to flow due to water film in liquefied deposits. Proceedings of the international conference on fast slope movement, Naples, May 2003.

[5] Beikae M. Is Newmark Method conservative? Proceedings of the fourth international conference on recent advances in geotechnical earthquake engineering, San Diego, March 2001. Paper No. 5.16, CD publication.

[6] Kokusho T, Motoyama R, Mantani S, Motoyama H. Seismic wave energy evaluation in surface layer for performance based design. 13th world conference on earthquake engineering, Vancouver 2004. Paper No. 3480.